PALEOCEANOGRAPHY, VOL. 21, PA4203, doi:10.1029/2005PA001200, 2006

The "African humid period" and the record of marine upwelling from excess ^{230}Th in Ocean Drilling Program Hole 658C

Jess Adkins,[1] Peter deMenocal,[2] and Gidon Eshel[3]

Received 26 August 2005; revised 4 February 2006; accepted 13 June 2006; published 20 October 2006.

[1] Using a high-resolution ^{230}Th normalized record of sediment flux, we document the deglacial and Holocene history of North African aridity and coastal upwelling at Ocean Drilling Program Hole 658C. At both the end of the Younger Dryas and after the 8.2 ka event, there are significant drops in terrigenous accumulation at our site, indicating an increase in the monsoon moisture flux over Africa at this time. At 5.5 ka, there is an abrupt end to the ''African humid period'' and a return to stronger upwelling conditions. For carbonate and opal fluxes the ^{230}Th normalization completely changes the shape of each record based on percentage variations alone. This site is a clear example of how variations in one sediment component can obscure changes in the others, and it demonstrates the need for radionuclide measurements more generally in paleoceanography. By taking our new records and a large amount of previous data from this site we conclude that increases in African moisture are tightly coupled to decreases in coastal upwelling intensity.

Citation: Adkins, J., P. deMenocal, and G. Eshel (2006), The ''African humid period'' and the record of marine upwelling from excess ^{230}Th in Ocean Drilling Program Hole 658C, *Paleoceanography*, *21*, PA4203, doi:10.1029/2005PA001200.

1. Introduction

[2] The record of deglacial changes in North African aridity is well documented in the literature. Early work on sand dune distribution [*Sarnthein*, 1978] and closed basin lake levels [*Street and Grove*, 1976], established the Last Glacial Maximum (LGM) as a time of hyperaridity in both the Sahara and Sahel region, whereas much of the present Saharan Desert was vegetated [*Jolly et al.*, 1998] and numerous lakes dotted the region during the early Holocene [*Gasse et al.*, 2000], or ''African humid period'' (AHP). Pollen records show that the classic AHP lasted from ~9 ka to ~6 ka [*Ritchie et al.*, 1985] but it is now clear that North African humidity probably started during the deglaciation, was interrupted by the Younger Dryas interval, and was well established by ~11 ka [*deMenocal et al.*, 2000a; *Gasse et al.*, 1990; *Street-Perrott and Perrott*, 1990].

[3] Climate models have shown that increased monsoon activity driven by an Early Holocene precessional summer insolation maximum was the main cause of the AHP, with related increases in tropical rainfall elsewhere across North Africa, the Arabian Peninsula, and south Asia. *Prell and Kutzbach* [1987] linked a planktonic foraminifera upwelling index record from the Arabian Sea to changes in precession over the last 140,000 years. However, their linear relationship between insolation anomalies and precipitation anomalies could not explain the abruptness or magnitude of the observed lake level increases. *Charney* [1975] was the first to postulate a vegetation-albedo feedback process in desert regions that would amplify insolation forced rainfall increases through the expansion of (light adsorbing) vegetation which lowers albedo and therefore inputs more energy into the monsoon system. This mechanism has been examined in many studies using very different models [*Ganopolski et al.*, 1998; *Liu et al.*, 2003] and this insolation-monsoon-vegetation feedback greatly amplifies the amount of rainfall for a given insolation change. Vegetation will also amplify a rainfall response through evapotranspiration as higher soil moisture and vegetation cover can lead to enhanced water vapor flux and latent heating of the atmosphere. This effect is strongly nonlinear in the midlatitudes [*Niyogi et al.*, 2002] and clearly affects the equilibrium solutions for simulations of the recent Sahel drought [*Wang and Eltahir*, 2000]. However, recent work has shown that the albedo feedback of vegetation cover has a larger effect on the large-scale circulation than the moisture flux effect [*Hales et al.*, 2004].

[4] Another possible feedback to explain the high lake levels, independent of vegetation, is increased sea surface temperatures (SSTs) in the monsoon moisture source region [*Kutzbach and Liu*, 1997; *Li and Philander*, 1997; *Liu et al.*, 2003]. In a coupled ocean-atmosphere model, an increase in SST off North Africa due to increased insolation forcing during the mid-Holocene is further amplified by an anomalous cyclonic wind pattern [*Ganopolski et al.*, 1998]. This atmospheric flow reduces the strength of the trade winds and their associated evaporative heat loss thus raising ocean temperatures. Higher SST then leads to greater precipitation over Africa because of both the circulation effect, the Intertropical Convergence Zone (ITCZ) moves farther north, and the large gradient in specific humidity between the ocean and land. In addition, detailed studies of the modern monsoon show both the vegetation-albedo feedback

[1]Department of Geological and Planetary Sciences, California Institute of Technology, Pasadena, California, USA.
[2]Lamont-Doherty Earth Observatory of Columbia University, Palisades, New York, USA.
[3]Department of Geophysical Sciences, University of Chicago, Chicago, Illinois, USA.

0883-8305/06/2005PA001200$12.00

and a variety of land-sea interactions can increase the variability, and potentially the mean state, of tropical monsoons [*Chou et al.*, 2000; *Zeng et al.*, 1999].

[5] Given the importance of the land-ocean interaction to insolation forcing of the monsoon, records that simultaneously monitor the windborne dust coming off of North Africa and the coastal upwelling system off North Africa could help to better understand the relationship between the AHP and surface ocean variability. We would like to understand the relationship between trade wind strength, North African vegetation, and SST/upwelling through time. Today northwestern Africa is dominated by the arid and semiarid expanses of the Saharan desert and the Sahel. The seasonal northward movement of the ITCZ in boreal summer, and the cyclonic inflow of moisture rich winds from over the ocean, creates a band of savannah grasslands that is easily seen in the NDVI SeaWiFS satellite product (Figure 1). This seasonal "greening" of the Sahel is accompanied by reduced upwelling in much of the coastal ocean south of 20°N. In boreal winter, the atmospheric circulation reverses and dry NE trade winds push farther to the south and there is strong upwelling along much of the coast of northwest Africa. The southward flowing Canary Current detaches from the NW African continental margin between 25° and 20°N and establishes strong year-round wind-driven upwelling in the vicinity of Cape Blanc, Mauritania [*Muller and Fischer*, 2001]. Upwelling is enhanced during boreal winter in association with the NE trade winds. During the early Holocene when much of the Sahara was wetter than today, there could have been large changes in both the seasonality and the mean strength of these trade winds. The resulting changes in the coastal upwelling signal should be recorded in marine sediments and, if properly interpreted, could increase our understanding of the feedback between terrestrial aridity and ocean SST.

[6] Sediments from Ocean Drilling Program (ODP) Hole 658C off Cape Blanc (20°45′N, 18°35′W, 2263 m, Figure 1) have been used to infer the integrated history of the AHP. While individual lake records can constrain when a local moisture threshold was crossed, marine sediments can faithfully monitor the areally integrated rates of change in the terrestrial moisture balance of the Saharan dust source region. A surprisingly abrupt increase in the percentage of terrigenous material at Site 658 indicates that the switch out of the AHP occurred at 5.5 ka and lasted only a few hundred years [*deMenocal et al.*, 2000a]. This mid-Holocene humid-arid transition has also been detected off East Africa and Arabia where the shift was apparently more gradual [*Fleitmann et al.*, 2003]. However, the use of component percentages in marine sediments can be misleading because the total sediment must always sum to 100%. Large changes in the flux of one sediment component to the site must induce inverse changes in the percentage of other components, even when their flux remained constant.

[7] In this paper we use high-resolution measurements of ^{230}Th, ^{232}Th and ^{238}U to constrain the history of both vertical and lateral sediment flux at Hole 658C over the last 18,000 years. The ^{230}Th normalized fluxes were developed to produce unbiased estimates of the component mass flux deposition [*Bacon*, 1984; *Suman and Bacon*, 1989]. The method is based on the fact that the instantaneous ratio of water column scavenged ^{230}Th flux to the total sediment flux must be equal to the concentration (in dpm/g) of ^{230}Th in the underlying sediment. The resulting equation is:

$$\text{normalized sediment flux} = \frac{\beta z}{\text{Ex. } ^{230}\text{Th}_0}(\text{f}_i)$$

The product of β, the production rate of ^{230}Th from ^{234}U in the water column (2.63×10^{-5} dpm/cm^3/kyr) and z, the water column depth, is the flux of excess Th to the sediment. Here excess ^{230}Th means that component of the total ^{230}Th not derived from detrital material or supported by ^{238}U decay within the sediments. Dividing this expected ^{230}Th flux by the measured concentration of initial excess ^{230}Th gives the total sediment accumulation rate. Multiplying by the fractional component of *i* then also yields the flux of component *i*.

[8] An important assumption in this method is that all of the ^{230}Th produced in the water column is efficiently scavenged to the seafloor, regardless of the total particle flux. A sediment trap calibration of this relationship showed that it is true within about 20% [*Yu et al.*, 2001] and this result was confirmed in an ocean GCM [*Henderson et al.*, 1999]. However, this variability is not random. Regions of high flux tend to scavenge ^{230}Th from the water column such that our site might overestimate the amount of ^{230}Th in the sediments at the high end of this range [*Francois et al.*, 2004]. Recently, *Luo and Ku* [2004] have argued that the distribution coefficient (K_d) for scavenging Th to particulate matter is heavily dependent on particle composition. Specifically, they argue that lithogenic particles have several orders of magnitude greater affinity for Th than do biogenic carbonate and opal particles. Considering a more global data set, *Chase and Anderson* [2004] and *Chase et al.* [2002] concluded that there is a roughly equal K_d for Th between clay and carbonate particles. These authors also found flaws in the earlier work and reinterpretation by Luo and Ku. As the carbonate and lithogenic percentages at our site differ by only a factor of 2 over all sediment depths, it is safe to assume that within the stated errors all of the ^{230}Th produced in the water column over site 658 is scavenged to the seafloor.

[9] Provided that lateral sediment transport along the ocean bottom does not change the ratio of ^{230}Th to total sediment, the $^{230}\text{Th}_{xs}$ method can also distinguish between vertical and horizontal accumulation. At discrete depths, the $^{230}\text{Th}_{xs}$ measurement reflects the basin wide vertical accumulation rate, integrated over the area from which sediments are focused. To calculate a sediment focusing factor (ψ) between well-dated depth intervals, the sum of the measured $^{230}\text{Th}_{xs}$ can be divided by the expected amount of Th solely due to vertical rain:

$$\psi = \frac{\int_{z_1}^{z_2} Ex.^{230}Th\rho dz}{\beta z(t_2 - t_1)}$$

When this number is less than one, there has been removal of sediment and ^{230}Th (winnowing) and when this number

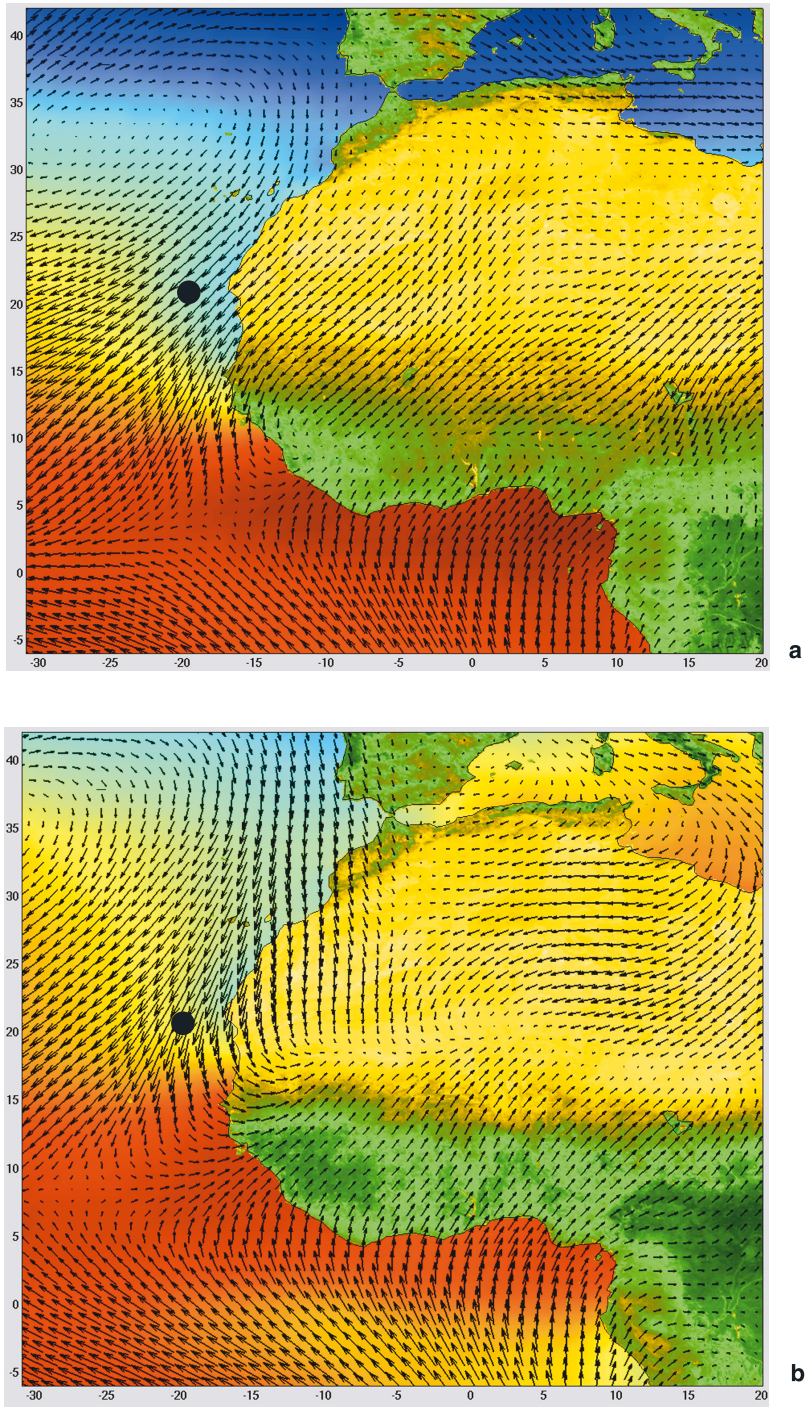

Figure 1. Location of ODP core 658C and relevant modern climatology. (a) Winter months (December, January, February). (b) Summer months (June, July, August). Color in ocean is sea surface temperature, and color on land is the normalized difference vegetation index satellite product (http://eos-webster.sr.unh.edu/data_guides/ndvi_dg.jsp). Vectors show wind direction and speed for that season. Upwelling favorable trade winds blow all year at the core site and to its north. Seasonally strong upwelling is driven by increased trade wind strength in the winter months and results in a larger region of cool waters to the south of the core site. Vegetation in the Sahel region is more productive in the summer monsoon months when the Intertropical Convergence Zone has moved to is maximum northward latitude, providing increased moisture flux in this season.

is greater than one there has been sediment and ^{230}Th added from a source other than rain through the water column (focusing). If the sediment transport process does not fractionate the major sediment components from one another, than the accumulation fluxes determined by the instantaneous excess ^{230}Th method are not changed. Finally, given thorium's insolubility in the water column and in pore waters, the $^{230}Th_{xs}$ concentration is a function of only the vertical sediment rain, regardless of diagenesis. However, any diagenetic removal of carbonate or opal will affect the measured fluxes of these components. The $^{230}Th_{xs}$ method is therefore a measurement of the accumulation in the sediment, rather than an estimate of rain through the water column.

2. Methods

2.1. Bulk Measurements

[10] Down-core carbonate and biogenic opal percentages from Hole 658C were determined as described by *deMenocal et al.* [2000a]. Terrigenous percentages were calculated as the residual from 100% of the carbonate and opal sum. Dry bulk density was calculated from the gamma ray attenuation porosity estimation (GRAPE) measurements made at sea. GRAPE values were calibrated from in situ dry bulk density measurements. As cores from Hole 658C were not split on board the drill ship, we used the Hole B calibration and applied it to the GRAPE data from Hole C. To minimize problems with small offsets in the different depth scales, the Hole B calibration was made using the mbsf scale for each bulk density measurement and the average of the GRAPE data within a 25 cm window around this depth. The resulting regression, with a 95% confidence interval on the slope, is

$$\text{estimated dry bulk density} = 1.75[\pm 0.57] \times \text{GRAPE} - 1.89 \quad \left(n = 20; r^2 = 0.62\right)$$

Foraminifera counts were performed as described by *deMenocal et al.* [2000b]. The depth scale adopted for this paper follows previous work on Hole 658C [*deMenocal et al.*, 2000b].

[11] Initial excess thorium measurements (n = 120) were made down core by complete digestion of ~0.7 g dry wt. sediment samples, anion exchange chromatography and Inductively Coupled Plasma–Mass Spectrometry (ICP-MS). The basic analytical procedure follows the original work that compared alpha-counting and ICP-MS detection schemes [*Shaw and Francois*, 1991]. However, enough changes were made in the procedure to warrant a more complete description here. Sediment digestion followed the procedure of *Anderson and Fleer* [1982] except that extra HF additions were used for these detrital rich sediments and samples were spiked with ^{229}Th before digestion. The digested sediment, contained in a perchloric acid drop, was taken up in 40 mL of 2N HCl and weighed. A 40 μl aliquot was removed for detrital U and Th determination, weighed, and spiked with ^{236}U and ^{230}Th. This aliquot was diluted with 2 mL of 1% HNO_3 and run on the ICP-MS. Weights were used to calculate the [^{238}U] and [^{232}Th] in the total sample and allowed us to use much less spike per sample. The bulk of the sediment solution was adjusted to pH~8 with NH_4OH and centrifuged for 15 min. Precipitates were washed with clean water, redissolved and centrifuged again.

[12] Precipitates from the digestion procedure were dissolved in HNO_3 and heated down to a small drop of solution. This drop was taken up in 8N HNO_3 and loaded onto a 5 mL nitric preconditioned anion exchange column (Dowex AG1-X8). The column was washed with 8N HNO_3 to remove salts and then eluted with 10 mL conc. HCl and 8 mL clean H_2O. Eluant was heated down to a single drop of liquid, taken up in a few milliliters of clean 1% HNO_3 and run on the ICP-MS.

2.2. Mass Spectroscopy and Calculations

[13] Samples were analyzed in peak jumping mode on the LDEO VG Plasma Quad 2 ICP-MS equipped with an auto sampler. The detrital fraction was run with a Meinhard nebulizer at standard flow and lens settings. Equal dwell times were used for ^{230}Th, ^{232}Th, ^{236}U and ^{238}U. Low-level ^{229}Th and ^{230}Th samples were run on the same machine with a VG Mistral nebulizer. In both cases a solution of known isotopic ratio was run to correct for machine mass bias effects. Rinse times between samples were between 3 and 5 min. Detrital samples were analyzed once while low-level Th data was collected in triplicate on the ICP-MS. Errors were calculated for individual samples by propagating 1σ estimates based on counting statistics through the various equations. Excess ^{230}Th is calculated according to the equation:

$$\text{Ex.}^{230}\text{Th} = {}^{230}A - 0.7x^{232}A - \left({}^{238}A - 0.7x^{232}A\right)x\,\text{age factor}$$

where activities (A) are in units of dpm/g. The terrestrial $^{230}A/^{232}A$ ratio of 0.7 is used to correct for detrital ^{230}A. Excess values of ^{230}A are calculated relative to nondetrital ^{238}A where secular equilibrium between ^{230}A and ^{238}A is assumed. This authigenic uranium is used to account for radiogenic ^{230}Th and it might have a seawater $^{234}U/^{238}U$ activity ratio of 1.15 instead of our assumed value of 1. However, the difference between the two does not change the calculated excess ^{230}Th within the stated errors. Our samples are too young for the 15% difference in authigenic U activity ratio to affect the calculated ^{230}Th data. Initial excess ^{230}A values are determined by decay correcting to the time of deposition based on the sediment age model. Counting statistics errors (Table 1) are generally <1% and represent valid error estimates as 7 of 8 replicates agreed within the 2σ range. The seven procedural blanks averaged below 0.01 dpm/g for ^{230}A.

3. Results

3.1. Age Model

[14] The 30 AMS dates used to construct an age model for Hole 658C have been reported previously [*deMenocal et al.*, 2000b]. As the timing of events and position of age

Table 1. Radionuclide Data for ODP Hole 658c

Depth, m	Age, years	^{230}Th, dpm/g	1 σ Error	^{232}Th, dpm/g	1 σ Error	^{238}U, dpm/g	1 σ Error	Excess ^{230}Th, dpm/g	1 σ Error
0.03	193	2.860	0.038	1.246	0.113	2.026	0.152	1.985	0.088
0.05	289	2.890	0.034	1.293	0.015	2.064	0.038	1.981	0.035
0.07	384	11.47	0.180	1.241	0.015	1.914	0.014	10.59	0.180
0.09	480	5.710	0.113	1.232	0.026	1.939	0.040	4.842	0.114
0.11	515	2.727	0.070	1.337	0.021	2.144	0.030	1.784	0.072
0.18	638	2.774	0.023	1.267	0.013	2.442	0.014	1.876	0.025
0.20	675	5.038	0.098	1.308	0.041	2.615	0.077	4.111	0.102
0.22	712	2.937	0.037	1.407	0.006	2.853	0.012	1.939	0.038
0.26	785	2.902	0.036	1.328	0.040	2.861	0.055	1.957	0.046
0.31	887	2.901	0.076	1.187	0.022	2.537	0.019	2.055	0.078
0.33	933	2.869	0.118	1.334	0.027	3.194	0.031	1.915	0.119
0.35	980	2.961	0.096	1.209	0.005	2.777	0.008	2.095	0.096
0.37	1027	2.972	0.032	1.395	0.016	3.156	0.047	1.973	0.034
0.42	1143	2.966	0.027	0.962	0.015	2.394	0.028	2.273	0.029
0.44	1190	2.924	0.064	1.348	0.013	3.250	0.023	1.953	0.064
0.46	1237	3.096	0.070	1.359	0.018	3.308	0.044	2.116	0.071
0.48	1283	2.979	0.040	1.389	0.028	3.206	0.053	1.978	0.045
0.51	1353	3.066	0.062	1.372	0.019	3.211	0.024	2.075	0.064
0.55	1515	2.937	0.114	1.380	0.018	3.234	0.040	1.937	0.115
0.57	1630	3.065	0.152	1.371	0.012	3.279	0.033	2.067	0.153
0.59	1745	3.029	0.019	1.314	0.040	3.237	0.075	2.069	0.034
0.61	1860	3.034	0.072	1.251	0.013	3.170	0.013	2.116	0.072
0.63	1975	2.883	0.082	1.371	0.027	3.562	0.053	1.872	0.084
0.67	2271	3.176	0.060	1.330	0.073	3.768	0.170	2.182	0.079
0.69	2452	2.939	0.010	1.257	0.021	3.414	0.080	2.000	0.018
0.71	2633	3.178	0.092	1.362	0.027	3.612	0.030	2.160	0.094
0.76	3085	3.032	0.087	1.304	0.025	3.724	0.056	2.042	0.089
0.78	3265	3.228	0.044	1.319	0.011	3.684	0.029	2.226	0.045
0.80	3446	3.151	0.093	1.308	0.023	3.765	0.083	2.151	0.095
0.82	3627	3.276	0.045	1.371	0.026	3.891	0.023	2.226	0.049
0.84	3808	2.983	0.110	1.239	0.013	3.541	0.060	2.030	0.110
0.86	3989	3.173	0.105	1.342	0.047	4.094	0.112	2.130	0.110
0.91	4322	3.280	0.030	1.343	0.015	3.963	0.062	2.232	0.032
0.93	4384	3.225	0.006	1.325	0.022	4.257	0.041	2.173	0.017
0.97	4507	3.200	0.062	1.163	0.020	3.629	0.059	2.275	0.063
1.04	4723	3.368	0.019	1.344	0.013	4.425	0.047	2.276	0.021
1.09	4878	3.293	0.073	1.412	0.023	4.423	0.058	2.145	0.075
1.11	4939	3.461	0.111	1.374	0.061	4.192	0.137	2.346	0.119
1.13	5001	3.417	0.020	1.395	0.026	4.348	0.086	2.276	0.027
1.15	5063	3.444	0.025	1.379	0.073	4.170	0.218	2.318	0.058
1.17	5125	3.297	0.114	1.405	0.028	4.195	0.060	2.149	0.116
1.19	5186	3.482	0.085	1.395	0.014	4.448	0.028	2.324	0.086
1.24	5372	3.559	0.021	1.382	0.008	4.131	0.033	2.417	0.022
1.26	5497	3.923	0.051	1.272	0.015	3.917	0.033	2.862	0.052
1.31	5808	4.015	0.130	0.994	0.013	3.857	0.038	3.131	0.131
1.35	6057	3.893	0.017	1.023	0.018	3.435	0.040	3.009	0.021
1.40	6369	3.974	0.098	0.993	0.017	3.442	0.068	3.100	0.099
1.42	6493	4.020	0.005	0.947	0.033	3.312	0.114	3.181	0.025
1.47	6805	4.072	0.029	0.974	0.006	3.233	0.059	3.213	0.029
1.49	6929	4.050	0.036	0.947	0.007	3.208	0.020	3.207	0.036
1.56	7365	4.051	0.081	0.889	0.029	3.331	0.140	3.226	0.084
1.61	7538	3.956	0.024	0.859	0.029	3.388	0.111	3.140	0.033
1.63	7570	4.026	0.119	0.889	0.019	3.340	0.068	3.195	0.120
1.65	7603	3.987	0.055	0.911	0.023	3.406	0.094	3.134	0.058
1.67	7635	4.010	0.064	0.811	0.013	3.013	0.073	3.251	0.064
1.69	7667	3.948	0.043	0.793	0.030	3.052	0.090	3.198	0.048
1.71	7699	3.902	0.033	0.889	0.035	3.320	0.121	3.067	0.042
1.73	7731	3.801	0.036	0.889	0.043	3.348	0.158	2.964	0.048
1.75	7763	3.927	0.014	0.895	0.034	3.400	0.124	3.081	0.030
1.77	7795	4.030	0.030	0.856	0.026	3.326	0.094	3.214	0.036
1.79	7828	3.916	0.046	0.884	0.013	3.558	0.084	3.063	0.047
1.81	7860	3.948	0.066	0.872	0.007	3.625	0.040	3.095	0.066
1.83	7892	3.901	0.027	0.852	0.031	3.593	0.145	3.063	0.037
1.89	8293	3.633	0.006	0.820	0.025	3.559	0.090	2.803	0.020
1.91	8528	3.127	0.025	0.825	0.022	3.736	0.102	2.273	0.031
1.93	8763	3.194	0.010	0.855	0.033	3.649	0.118	2.323	0.027
1.95	8998	3.156	0.043	0.807	0.091	3.464	0.425	2.326	0.086
1.97	9233	3.133	0.032	0.855	0.038	3.821	0.138	2.234	0.044
1.99	9468	3.222	0.051	0.796	0.067	3.723	0.287	2.363	0.074
2.06	10037	3.143	0.034	0.821	0.033	3.746	0.131	2.250	0.043
2.08	10146	3.152	0.053	0.845	0.042	3.553	0.171	2.261	0.064

Table 1. (continued)

Depth, m	Age, years	^{230}Th, dpm/g	1 σ Error	^{232}Th, dpm/g	1 σ Error	^{238}U, dpm/g	1 σ Error	Excess ^{230}Th, dpm/g	1 σ Error
2.10	10254	3.185	0.006	0.820	0.043	3.627	0.200	2.299	0.037
2.12	10363	3.200	0.066	0.805	0.012	3.687	0.069	2.315	0.067
2.14	10471	3.122	0.010	0.856	0.025	3.741	0.112	2.195	0.024
2.16	10580	3.323	0.016	0.839	0.046	3.491	0.183	2.430	0.041
2.18	10689	3.177	0.030	0.852	0.043	3.755	0.184	2.245	0.047
2.20	10797	3.156	0.041	0.942	0.018	4.236	0.029	2.113	0.043
2.22	10906	3.078	0.036	1.032	0.009	4.086	0.027	1.992	0.036
2.24	11014	3.111	0.065	0.861	0.019	3.792	0.027	2.159	0.066
2.26	11123	3.108	0.063	0.942	0.012	3.958	0.022	2.085	0.064
2.32	11407	3.109	0.021	0.907	0.018	3.942	0.067	2.100	0.025
2.34	11473	3.069	0.015	0.890	0.012	3.928	0.018	2.069	0.017
2.36	11540	3.081	0.004	0.893	0.009	3.722	0.026	2.101	0.008
2.38	11606	3.029	0.006	0.937	0.012	3.764	0.033	2.014	0.011
2.40	11673	3.096	0.077	0.840	0.031	3.395	0.119	2.182	0.081
2.42	11739	3.112	0.022	0.914	0.020	3.634	0.033	2.121	0.027
2.44	11806	2.997	0.100	0.865	0.009	3.592	0.016	2.039	0.100
2.46	11872	3.051	0.043	0.944	0.007	3.770	0.010	2.021	0.043
2.48	11939	3.037	0.062	0.947	0.009	3.802	0.068	1.999	0.063
2.50	12005	3.058	0.063	0.988	0.016	3.928	0.066	1.977	0.065
2.57	12238	2.708	0.032	0.945	0.010	4.176	0.029	1.614	0.033
2.62	12404	2.464	0.081	1.117	0.014	4.404	0.056	1.229	0.082
2.64	12471	2.530	0.041	1.039	0.021	4.188	0.039	1.367	0.044
2.66	12538	2.596	0.093	1.068	0.008	4.401	0.065	1.386	0.094
2.68	12604	2.653	0.078	1.058	0.021	4.110	0.011	1.483	0.080
2.70	12671	2.712	0.067	0.978	0.022	3.917	0.050	1.613	0.069
2.72	12737	2.658	0.023	0.951	0.011	4.364	0.045	1.515	0.025
2.74	12804	2.571	0.080	1.045	0.019	4.484	0.065	1.350	0.082
2.80	12990	2.680	0.032	0.997	0.008	4.426	0.027	1.490	0.032
2.82	13030	2.592	0.030	1.047	0.033	4.291	0.107	1.387	0.041
2.84	13070	2.634	0.025	0.968	0.013	4.114	0.050	1.500	0.027
2.86	13110	2.700	0.036	0.901	0.015	4.418	0.079	1.561	0.039
2.88	13150	2.726	0.079	0.896	0.022	4.402	0.064	1.590	0.081
2.90	13190	2.692	0.050	0.837	0.011	3.989	0.046	1.640	0.051
2.92	13230	2.679	0.006	0.954	0.011	4.065	0.034	1.550	0.011
2.94	13270	2.584	0.013	0.949	0.061	4.101	0.274	1.449	0.059
2.96	13354	2.900	0.037	0.905	0.014	4.030	0.020	1.798	0.038
2.98	13438	2.730	0.038	0.899	0.007	4.150	0.036	1.612	0.038
3.00	13523	3.039	0.034	0.911	0.006	4.142	0.022	1.910	0.035
3.02	13607	3.033	0.114	0.962	0.004	4.200	0.039	1.861	0.114
3.10	13944	2.850	0.076	0.939	0.009	4.271	0.020	1.667	0.076
3.12	14028	2.890	0.046	0.951	0.014	4.384	0.070	1.680	0.048
3.14	14095	2.908	0.126	0.925	0.010	4.183	0.054	1.742	0.127
3.16	14146	2.793	0.035	0.949	0.016	4.316	0.040	1.590	0.040
3.18	14197	2.841	0.105	0.867	0.012	4.145	0.027	1.717	0.106
3.20	14248	2.783	0.035	0.821	0.013	3.903	0.055	1.723	0.038
3.25	15118	2.339	0.046	0.861	0.008	3.392	0.018	1.316	0.047
3.29	17505	2.792	0.048	1.068	0.022	3.294	0.064	1.610	0.050
3.31	17675	3.050	0.059	1.045	0.012	3.415	0.059	1.850	0.061
3.33	17844	2.885	0.053	1.136	0.019	3.283	0.035	1.650	0.055
3.35	18012	2.827	0.067	1.060	0.008	3.130	0.046	1.661	0.068
3.37	18179	2.921	0.071	1.122	0.029	3.278	0.069	1.690	0.075
3.39	18347	2.961	0.065	1.066	0.009	3.145	0.031	1.786	0.066
3.41	18515	2.924	0.090	1.079	0.008	3.211	0.030	1.730	0.090

control points are important in much of the discussion below, we plot the planktonic foraminifera ^{14}C data in Figure 2. Raw data from *G. bulloides* and *G. inflata* have been adjusted for a 500-year reservoir correction because of the influence of "older" surface waters at this upwelling site. This reservoir correction may have changed in the past associated with variations in regional upwelling. These ^{14}C ages were converted to calendar ages using the Calib 4.12 program [*Stuiver and Reimer*, 1993]. Where foraminiferal pairs exist from the same depth, the *G. inflata* data is generally younger. This behavior is expected in light of the tendency of *G. bulloides* to dominate the assemblage during the strong upwelling season. We construct the age model by using *G. inflata* data where available, except at 121 cm where the *G. bulloides* point is used to ensure consistency in the age model across the transition from the African humid period. Three *G. bulloides* dates (circled with dashed lines in Figure 2) that were run on the same day at the accelerator and resulted in age reversals were not used in the age model. The final depth versus age relationship is the gray line in Figure 2.

3.2. Percentages and Fluxes

[15] Bulk sediment percentages are shown in Figure 3. It is clear that the opal percent record does not follow the percent terrigenous pattern. The biogenic opal method

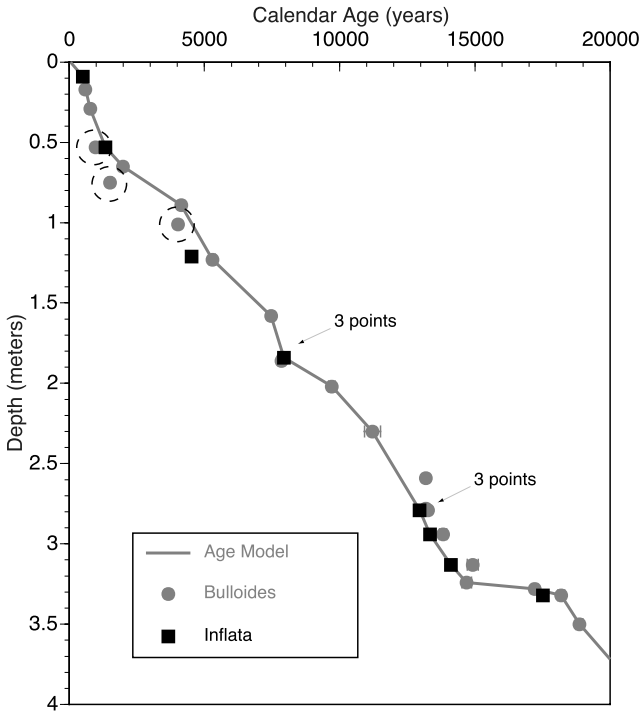

Figure 2. ODP Hole 658C age model. Planktonic foraminifera radiocarbon dates are shown for *G. Bulloides* and *G. Inflata* species following [*deMenocal et al*. [2000b]. Three points left out of the age model because of problems with that day's run on the accelerator mass spectrometry are shown with dashed circles. In general, the age model follows the youngest radiocarbon date at any depth with multiple measurements.

exploits the different solubilities of biogenic and terrigenous Si into a hot 2M $NaCO_3$ solution. At low opal and high terrigenous concentrations this method may bias the percent biogenic silica measurements toward higher values [*Mortlock and Frolich*, 1989]. However, our data do not show evidence of this problem. In fact there are several places where the biogenic opal signal rises while the terrestrial fraction is falling (~325 cm) and where the opal drops while the terrigenous percentage is constant (~180 cm).

[16] The use of the ICP-MS analytical method, where many samples can be run precisely and quickly, allows us to realize the potential of $^{230}Th_{ex}$ to capture short-term fluctuations in sediment accumulation rates and to differentiate flux changes between the various bulk sediment components. Our 120 down-core measurements of three separate radionuclides are shown as profiles in Figure 4 and in Table 1. There are significant changes in ^{230}Th concentration at 124 and 190 cm depth with two very large increases at 20 cm (one point) and 7–9 cm (two points). We can find no analytical reason to disregard these points. All three show large amounts of ^{230}Th without corresponding ^{232}Th, so increased blank Th is not likely. Except at 124 cm, these shifts are not seen in the ^{232}Th or the ^{238}U data. The $^{230}Th_{ex}$ record is largely determined by the measured ^{230}Th concentrations. Detrital ^{232}Th accounts for most of the ~1 dpm/g offset between the measured and calculated data (Table 1). Authigenic U (gray points in Figure 4c) does not vary systematically with initial excess ^{230}Th and contributes little to the calculated ^{230}Th number because this sediment is too young to have significant ingrowth of ^{230}Th from ^{238}U derived from seawater. A standard made from homogenized equatorial Pacific sediments was run seven times

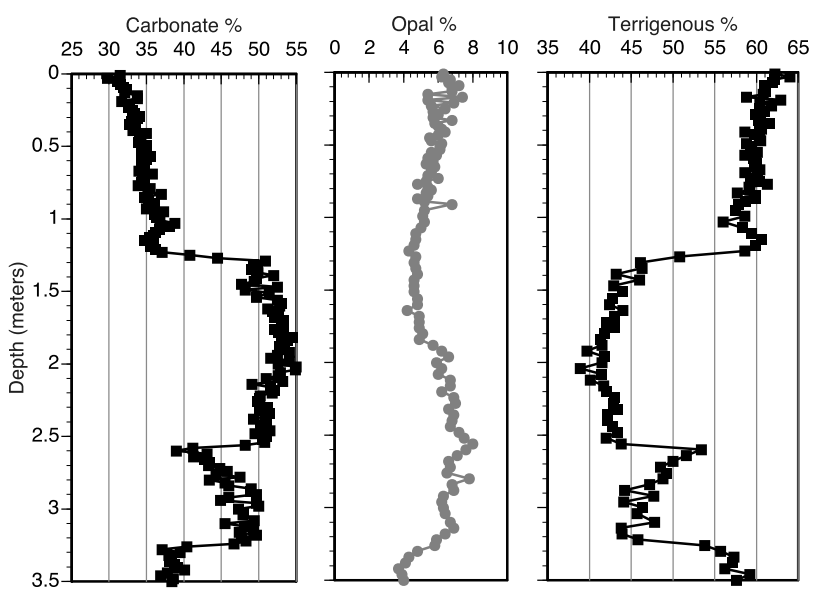

Figure 3. Bulk sediment percentages in ODP Hole 658C. Data are from *deMenocal et al.* [2000a]. Carbonate and terrigenous percents are mirror images of each other and indicate that changes in the flux of one species are probably driving changes in percent of the other. Percent organic carbon also varies down core between 1 and 2% but is not large enough to affect our flux calculations.

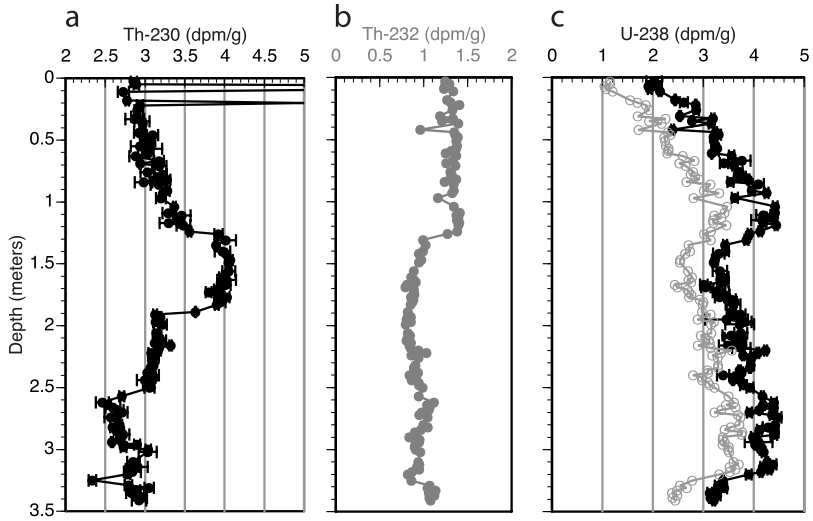

Figure 4. U series radionuclide data for ODP Hole 658C: (a) ^{230}Th, (b) ^{232}Th, and (c) ^{238}U. Error bars reflect propagated counting statistics. Excess ^{230}Th is principally driven by the measured ^{230}Th data. The ^{232}Th has one step change at ~124 cm and is generally 1/3 to 1/4 of the ^{230}Th value. Authigenic ^{238}U at this site (gray points in Figure 4c) is a few dpm/g, but the sediments are too young to contribute much ^{230}Th to the data.

during the sample processing. Initial $^{230}Th_{ex}$ values for this standard varied by less than 2.5% (2σ).

4. Discussion

4.1. Accumulation Rates and Sediment Focusing

[17] At ODP Site 658C the carbonate and terrigenous percent records are essentially mirror images of each other since they are the two dominant components (Figure 3). This behavior is a strong indication that one of the components has been diluted by the other, so that one or both of these records do not reflect the true history of accumulation at this site. Figure 5 shows that the relative sense of the terrigenous percent record is preserved when converted to normalized fluxes. In contrast, the carbonate data become markedly different when expressed as normalized fluxes rather than as percentages. The clear implication here is that variations in terrigenous material obscure the true carbonate accumu-

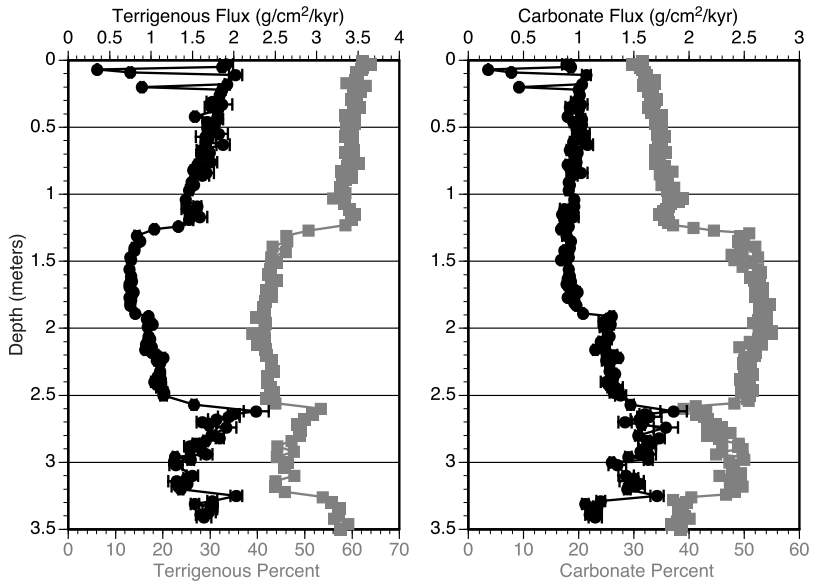

Figure 5. Comparison of percentage and accumulation flux for terrigenous and carbonate material in ODP Hole 658C. Excess-^{230}Th-normalized fluxes of terrigenous sediment generally have the same shape as the percentage data, indicating that previous interpretations of dust variability based on percent alone are probably correct. Carbonate fluxes are very different from the percent data, indicating that the large changes in terrigenous accumulation drive variations in percent $CaCO_3$.

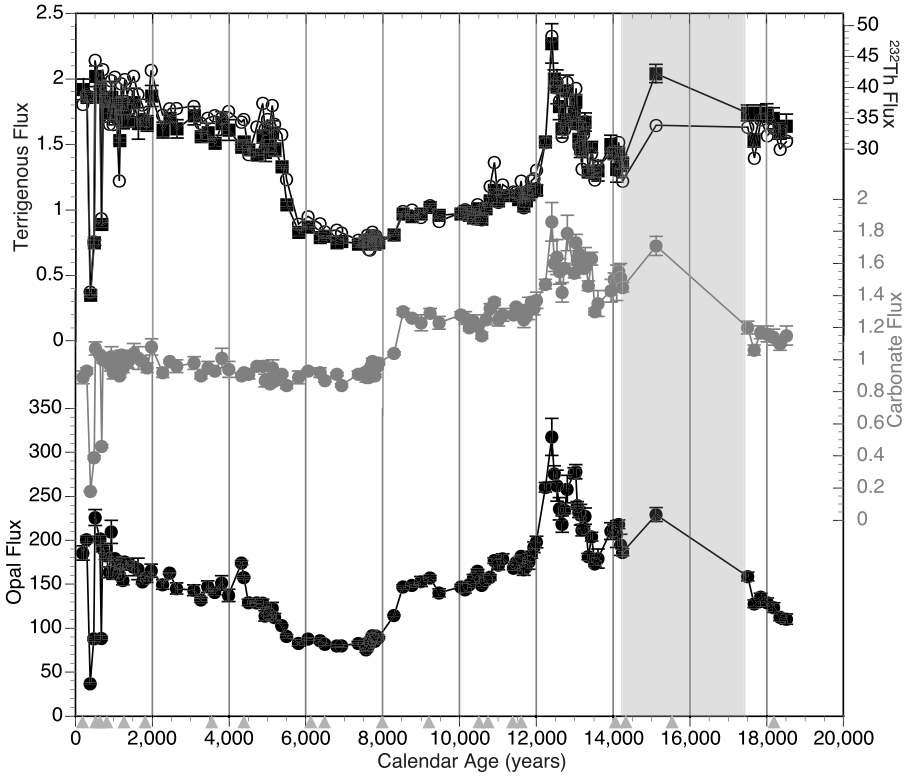

Figure 6. Excess ^{230}Th normalized fluxes of terrigenous (g/cm^2/kyr), carbonate (g/cm^2/kyr), and silicate (mg/cm^2/kyr) material at ODP Hole 658C plotted versus calendar age. The shape of each accumulation rate record largely follows the record of changes in the total flux. The "African humid period," as recorded by terrigenous flux at this site, has two distinct periods from the end of the Younger Dryas to ~8.2 ka and from ~8.2 ka to its abrupt end at 5.5 ka. Silicate and carbonate are made up of marine diatoms and coccoliths and therefore record the history of the coastal upwelling system off North Africa over the last 20,000 years. The region around 16 ka represents a time hiatus where sediment has been winnowed from this site. The ^{232}Th flux (mdpm/cm^2/kyr) is plotted as open circles and compared to the terrigenous flux. These two independent ways of calculating the detrital component of the sediments give virtually the same result. The gray area spans a time of sediment winnowing at this site and represents a portion of the time series that may be compromised.

lation history. Across 124 cm, where the $CaCO_3$ accumulation is constant, the transition to lower percent $CaCO_3$ is driven by a twofold to threefold increase in terrigenous supply. Similarly, a decrease in $CaCO_3$ flux at ~260 cm is masked in the percentage record as an increase because of a sharp drop in terrigenous flux as well. The constant %$CaCO_3$ across ~190 cm conceals a drop in carbonate accumulation because the terrigenous accumulation drops at this same time. All three of these events in the Th-normalized $CaCO_3$ accumulation record reflect significant climatic and oceanographic changes (see below) that would be misinterpreted without the Th normalization technique. Records of climate variability based on sediment percentages can be very misleading because the total must always sum to 100%. However, variations in terrigenous percentage preserve the shape of the accumulation flux curve so the percent record is therefore a reliable indicator of the abruptness and timing of the African humid period [*deMenocal et al.*, 2000a].

[18] With the use of our high-resolution age model and all the percentage data, we can calculate the flux of accumulating terrigenous, carbonate and opal material at Site 658 over the last 20,000 years (Figure 6). Contrary to the records of percentage, the three flux time series look remarkably similar, and several important shifts are now evident. First, rather than being a single event the "African humid period" clearly has several stages. Low terrigenous fluxes are first seen during the Bølling-Allerød, but this implied African humidity is interrupted by the Younger Dryas. The largest amplitude decrease in wind blown dust to our site occurred abruptly at 12.0 ka but we believe this date could really be the end of the Younger Dryas as our 500-year reservoir correction may not be large enough for this time interval [*Siani et al.*, 2001; *Waelbroeck et al.*, 2001]. With our new record, maximum humidity in North Africa as implied by the low terrigenous fluxes, occurred between 5.5 and 8.2 ka, corresponding to the end of Mediterranean sapropel 1 and its interruption with better ventilated waters in the early Holocene. The raw planktonic radiocarbon ages from Ba/Al data in Mediterranean Sea cores imply a slightly older age for the end of S1 [*Mercone et al.*, 2000], but *Rohling et al.* [2003] argue this age is actually younger because of bioturbation and that the sapropel signal is coincident with the

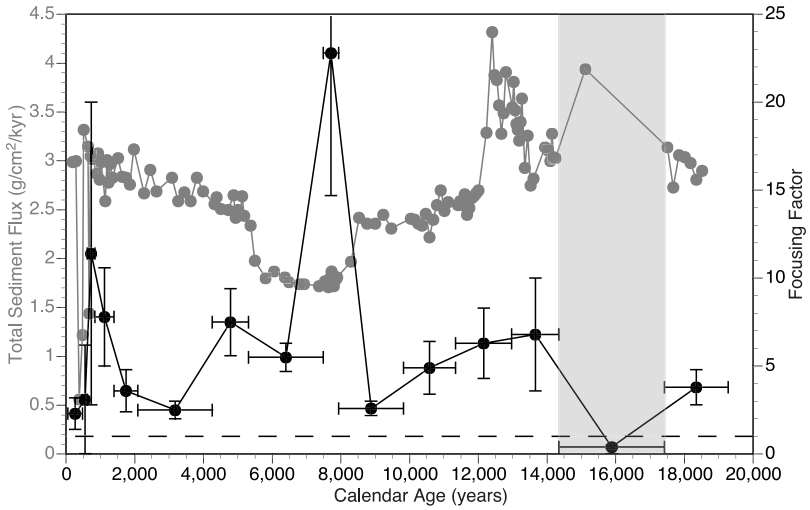

Figure 7. Total vertical sediment accumulation and lateral focusing at ODP Hole 658C. Focusing factors are calculated from the ratio of integrated excess ^{230}Th to expected excess ^{230}Th between well-dated sediment horizons. Outside of a period of winnowing from 14.5 to 17.5 ka this site receives a large amount of laterally transported sediment. The largest focusing value of ~20 just after 8.2 ka is well constrained by two radiocarbon dates at 150 and 180 cm. Our confidence in both the lateral and vertical sediment histories is increased because neither record looks like the other. The gray area spans a time of sediment winnowing at this site and represents a portion of the time series that may be compromised.

5.5 ka event seen in Greenland ice core K^+ data [*Mayewski et al.*, 1997]. Rohling et al. also assign an age of 8.4 ka to the interruption of Mediterranean dysoxia represented by S1 that is consistent with the age of the Ba/Al signal [*Mercone et al.*, 2000].

[19] More generally, all of the major sedimentary components decreased abruptly at around 8.2 ka indicating a strong teleconnection between African aridity, the North African upwelling system and high-latitude meltwater discharge into the North Atlantic from the final breaching of Lake Agassi [*Alley and Agustsdottir*, 2005]. The signal at 8.2 ka in our data is not seen in the sediment percentages because all three components decrease together, obscuring the change in accumulation rate. These 5.5 and 8.2 ka shifts are felt far afield in the Mediterranean region; in Swiss peat bogs [*Shotyk et al.*, 2002], Med pollen [*Magri and Parra*, 2002], Antarctic sea ice [*Hodell et al.*, 2001], Med Sapropels [*Rohling*, 1994], Red Sea salinity [*Arz et al.*, 2003], and dust off of Somalia [*Jung et al.*, 2004]. However, as opposed to the classic "8.2 ka event," our record shows a prolonged shift to wetter values after the Northern Hemisphere glacial melting. A recent compilation of many early Holocene records argues that monsoon indices in general show a trend to increased aridity earlier than the canonical 8.2 ka age of the North Atlantic meltwater event [*Rohling and Palike*, 2005]. Indeed the long duration of many tropical "8.2" events (from 8.4 to 7.9 ka) implies that a simple high-latitude forcing and tropical response model may be too simple.

[20] As a final check on our interpretation of the sediment fluxes, our terrigenous record is also compared to the flux of ^{232}Th in Figure 6 (open circles, in mdpm/g/cm^2). These two independent markers of detrital accumulation at site 658 give the same result and increase our confidence in measuring terrigenous percentage by difference from carbonate and opal measurements. There is also a clear difference in the response of carbonate and opal accumulation across the 5.5 ka transition to a drier North Africa. These changes in the upwelling dynamics at site 658 were hidden in the percent records and will be discussed further in a separate section below.

[21] In addition to the very different shape of the sediment component records, our new normalized fluxes differ greatly from the magnitude of previously published fluxes. Terrigenous fluxes based on the traditional method of multiplying the percent data by the sedimentation rate and the dry bulk density vary between about 7 and 12 g/cm^2/kyr [*deMenocal et al.*, 2000a]. These elevated values are not representative of the true vertical flux at this site but are instead due to the combination of sediment focusing and vertical particle fluxes [*Ruddiman*, 1997]. Modern sediment trap data near our site give a seasonal range of 1.1–2.0 g/cm^2/kyr, in good agreement with our core top value of 1.9 g/cm^2/kyr [*Ratmeyer et al.*, 1999]. Our large number of radiocarbon dates combined with the radionuclide data let us calculate the ratio between the ^{230}Th found in a sediment depth interval to the ^{230}Th expected from production in the overlying water column (see section 1). This record of lateral focusing is shown in Figure 7. In general, Site 658C receives over 3 times more sediment laterally as it does vertically, with large variability around this approximate average. In the sedimentation rate method of calculating accumulation rates this focused sediment is accounted for as if it were all coming from directly above the core site and will lead to overestimates of the vertical flux. Our focusing calculation does not account for any lateral transport of ^{230}Th in the water column, but this effect, if present at this high-flux site, is on the order of 20–30%

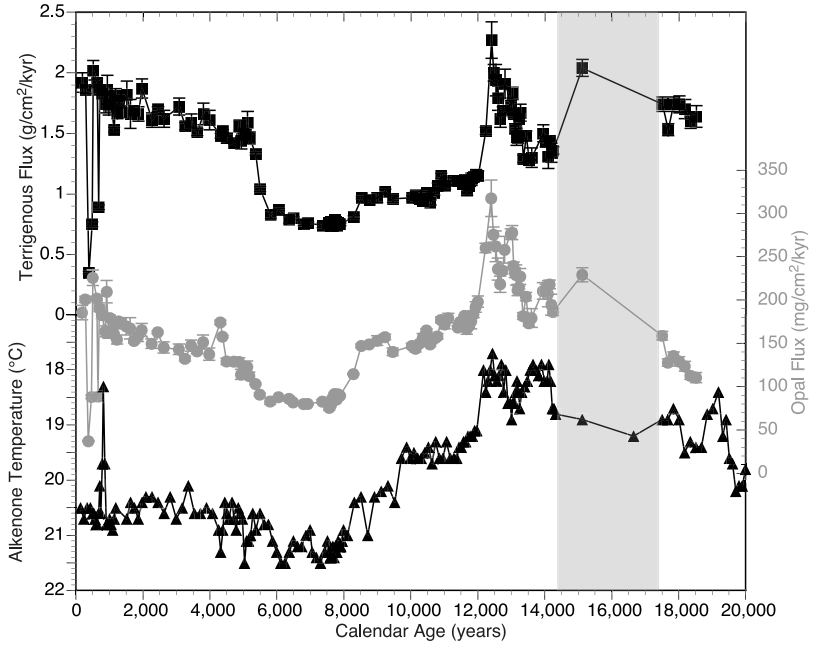

Figure 8. Alkenone SST, opal accumulation flux and terrigenous accumulation flux since the LGM. The strong covariance between the alkenone and opal records is a good indication that each of them represents the relative history of upwelling strength at this site over time. Biomarker temperatures are ~1°C warmer during the "African humid period" than during the late Holocene. Opal fluxes are at their minimum values from 8.2 to 5.5 ka. The gray area spans a time of sediment winnowing at this site and represents a portion of the time series that may be compromised.

[*Francois et al.*, 2004] and cannot explain the very large changes in focusing factor we document in Figure 7.

[22] Two separate times of increased sedimentation rate demonstrate the value of the $^{230}Th_{ex}$ measurements. At 7.9 ka a focusing factor above 20 is driven by two well resolved points in the age model where the sedimentation rate jumps to 62 cm/kyr. Site 658 has a similarly high sedimentation rate during the Younger Dryas (50 cm/kyr) but the focusing factor is much lower (5–8). These would both be times of high accumulation rate as calculated by the traditional method, but total vertical Th-normalized sediment flux is low at 7.9 ka and high during the Younger Dryas (Figure 7). While there is still a large amount of lateral sediment transport during the Younger Dryas, the ratio of Ex ^{230}Th found to the amount expected is smaller than for the brief interval around 7.9 ka and the greater vertical flux can be resolved. Finally, the focusing data reveal a distinct hiatus between ~14.4 and ~17.4 ka where sediment was winnowed from this site. Our confidence in both the records of vertical and lateral flux is increased because there is no systematic relationship between the two curves. Instantaneous vertical fluxes calculated from single $^{230}Th_{ex}$ points are separate from the integrated focusing flux calculated from $^{230}Th_{ex}$ inventories between radiocarbon dated horizons [*Bacon*, 1984].

4.2. Upwelling Variations and Links to African Climate

[23] Our Th normalized fluxes confirm and expand previous results about the African humid period based on terrigenous percent at Site 658 [*deMenocal et al.*, 2000a]. However, the normalized flux record is very different from the percent record for carbonate and opal. Because the bulk of these two sediment components are from coccoliths and marine diatoms respectively, these new flux records allow us to better interpret the history of upwelling off of North Africa. In addition, the whole data set together permits comparison of variability in the African monsoon to variability in the intensity of upwelling. An important caveat to this interpretation is that we can only constrain the burial flux of carbonate and opal. The true rain to the seafloor is potentially obscured by dissolution, especially for $CaCO_3$. However, the covariance of both biogenic species through most of the record is a strong indication that our data reflect the productivity of the waters above and not the dissolution strength of the waters at the sediment interface.

[24] Our flux data imply that changes in African aridity were closely tied to changes in coastal upwelling. The lowest biogenic accumulation rates occurred during the African humid period when terrigenous fluxes were also lowest (Figure 6). Similarly, the much more arid conditions of the Younger Dryas were associated with greater upwelling as indicated by the increased biogenic carbonate and opal fluxes. Our [^{238}U] data also hint at an increase in upwelling after 5.5 ka. The ~1 dpm/g drop in Uranium over the AHP and the abrupt increase at 5.5 ka (Figure 4) are both larger than variations in detrital Uranium based on the ^{232}Th content of the sediments. These authigenic uranium data support the idea of gradually decreasing organic carbon rain over the AHP followed by a large increase at the 5.5 ka event.

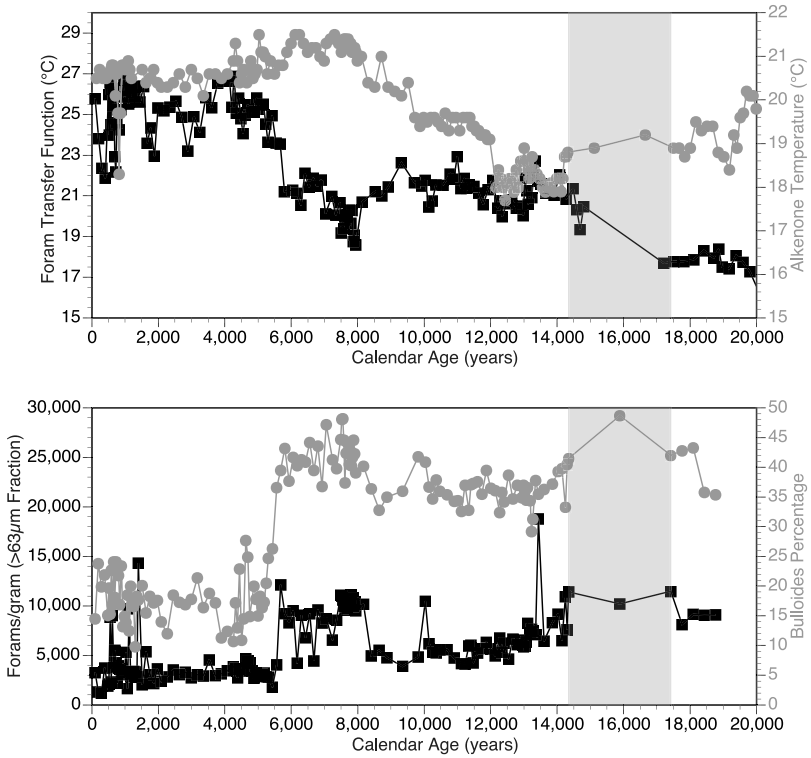

Figure 9. (a) Records of sea surface temperature at ODP Hole 658C. Alkenone (circles) and planktonic foraminifera transfer function (squares) based SST are shown. Both records show general warming since the Last Glacial Maximum, but the transfer function signal is much larger. Foraminifera species assemblages imply an ~4°C cooler SST during the AHP, while the biomarker record shows elevated temperatures during the early Holocene. (b) *Bulloides sp.* percentage data and the number of forams greater that 150 μm/g of sediment. The number/gram increase from 8.2 ka to 5.5 ka is mostly due to an increase in the *Bulloides* tests during a time when they have a slight increase in relative abundance. The gray area spans a time of sediment winnowing at this site and represents a portion of the time series that may be compromised.

[25] An independent confirmation of this proposed link between African climate and regional upwelling is provided by an alkenone SST record which was also measured at Site 658 [*Zhao et al.*, 1995]. Comparison of the Site 658C Th-normalized terrigenous and biogenic opal fluxes with the alkenone-derived SST record demonstrates the very close correspondence between the SST and opal flux upwelling proxies and the terrigenous flux proxy for NW African climate changes (Figure 8). A 4-year sediment trap calibration of alkenone-derived SSTs was conducted for the Cape Blanc region [*Muller and Fischer*, 2001]. These results have shown that flux-weighted alkenone SST estimates closely follow modern mean annual SSTs for the trap locations (22.1°C), and that this signal is preserved in core top sediments despite variable oxic diagenesis. The overall correspondence between the alkenone SST and Th-normalized flux data shown in Figure 8 provides compelling evidence linking the deglacial and Holocene evolution of NW African climate and coastal upwelling. Our flux based inferences of weaker upwelling during the AHP are in direct contrast to foram- and radiolarian-based upwelling indices [*Haslett and Smart*, 2006]. Our resolution to this difference is presented below.

[26] It has been noted previously that alkenone and foraminiferal transfer function SST estimates off NW Africa differ markedly across the deglacial transition [*Chapman et al.*, 1996; *deMenocal et al.*, 2000b; *Mix and Ruddiman*, 1986; *Zhao et al.*, 1995]. Alkenone SST estimates for this region are closely linked to the evolution of North Atlantic climate, with a pronounced expression of Younger Dryas cooling, followed by warmest conditions during the early Holocene and gradual cooling toward the present. Transfer function SST estimates on these same cores suggest that SSTs remained cool throughout the deglacial transition until the early Holocene (5.5 ka), after which SSTs were warmer (Figure 9a). An additional distinction is that the foram-based SST estimates commonly reveal century-millennial-scale SST cooling events within the Holocene, whereas the alkenone-derived records do not [*deMenocal et al.*, 2000b; *Kim et al.*, 2002; *Zhao et al.*, 1995].

[27] What is the reason for these differences? *Chapman et al.* [1996] proposed that the discordance between these two SST proxies was related to shifts in seasonal fluxes of the organic versus particulate sediment fluxes. However, at Site 658, the persistence of cooler SSTs across the deglacial and into the early Holocene is nearly entirely attributable to high

percentages of *G. bulloides* (Figure 9b). This species is uniformly abundant from the Younger Dryas until the 5.5 ka event and therefore keeps the transfer function SSTs artificially low. The *G. bulloides* specimens were also noticeably larger during this early Holocene "cool" period as indicated by the increase of the number of forams larger than 63 μm (Figure 9b). This early Holocene period is when the alkenone and foraminifera transfer function are most offset. Hence the difference between the transfer function and alkenone SSTs at this location may be due to factors regulating the size and abundance of *G. bulloides* that are independent of SST, and therefore do not affect the response of the alkenone saturation ratio to temperature (though physiological effects on alkenones have been reported recently [*Prahl et al.*, 2003]. Specifically, enhanced river nutrient supply during the African humid period may have contributed to the increased early Holocene abundances and size of *G. bulloides*, resulting in apparently cooler transfer function SSTs. In contrast, the century-millennial-scale SST variations within the Holocene that have been linked to North Atlantic cooling events [*Bond et al.*, 1997, 2001] reflect variations in the relative proportions of *N. pachyderma* (dextral) and *G. inflata* which are interpreted to reflect variations in the southward penetration of the cooler Canary Current waters [*deMenocal et al.*, 2000b]. Therefore millennial-scale temperature changes estimated by foraminifera abundance patterns would not be sensitive to the *G. bulloides* abrupt shift in the early Holocene and probably are a robust measure of millennial-scale temperature change.

[28] Overall, our new data and the reinterpretation of the two SST proxies lead to a consistent relationship between African aridity and upwelling at site 658 across the deglaciation and through the Holocene. Alkenone SSTs gradually warm from the end of the Younger Dryas until the 5.5 ka event. This pattern is consistent with decreasing opal and carbonate fluxes and lower authigenic uranium concentrations due to the reduced upwelling intensity. At the same time northwest Africa becomes wetter showing marked shifts to more humidity at the end of the Younger Dryas and at 8.2 ka. Foraminiferal transfer functions are biased by a non-SST related effect on *G. bulloides* percentages that also makes this species precipitate larger tests. Millennial-scale SST variations derived from foram species abundances, on the other hand, are based on the mirror image abundance pattern of *N. pachyderma* and *G. inflata*. This result should not be affected by a step function change in *G. bulloides* abundance at 5.5 ka.

5. Conclusions

[29] Our high-resolution record of ^{230}Th normalized terrigenous flux confirms an earlier conclusion, based on sediment percentages at ODP 658C, that the AHP ended abruptly at ~5.5 ka. These data also demonstrate that there is a large amount of lateral sediment focusing at this site, outside of a period during the deglaciation where winnowing removed sediment. This focusing obscures the record of biogenic production as recorded by sediment percentages of carbonate and opal. After ^{230}Th normalization, the terrigenous, carbonate and opal fluxes have similar shapes. Normalized fluxes all show a decrease at ~8.2 ka, that was lacking in the percentage data, and indicate a teleconnection between the low latitudes and the glacial meltwater discharge from Lake Agassi at this time. The tight correspondence between terrigenous and opal fluxes with alkenone SST estimates indicate that there is a strong link between African aridity and the North African upwelling system. Overall, it is clear that ^{230}Th normalization is an important tool for reconstructing paleofluxes of sedimentary material.

[30] **Acknowledgments.** We thank Joe Ortiz for his analysis of the bulk density data and for conversations over the years. Two anonymous reviewers improved the clarity of the manuscript. J.F.A.'s work was supported by a LDEO postdoctoral fellowship and by the Lamont Climate Center. NSF grant OCE-0318445 supported J.F.A.'s work on this project at Caltech.

References

Alley, R. B., and A. M. Agustsdottir (2005), The 8k event: Cause and consequences of a major Holocene abrupt climate change, *Quat. Sci. Rev.*, *24*, 1123–1149.

Anderson, R. F., and A. Fleer (1982), Determination of natural actinides and plutonium in marine particulate material, *Anal. Chem.*, *54*, 1142–1147.

Arz, H. W., et al. (2003), Mediterranean moisture source for an Early-Holocene humid period in the northern Red Sea, *Science*, *300*, 118–121.

Bacon, M. P. (1984), Glacial to interglacial changes in carbonate and clay sedimentation in the Atlantic Ocean estimated from ^{230}Th measurements, *Isotope Geosci.*, *2*, 97–111.

Bond, G., et al. (1997), A pervasive millennial-scale cycle in North Atlantic Holocene and glacial climates, *Science*, *278*, 1257–1266.

Bond, G., et al. (2001), Persistent solar influence on North Atlantic climate during the Holocene, *Science*, *294*, 2130–2136.

Chapman, M. R., N. J. Shackleton, M. Zhao, and G. Eglinton (1996), Faunal and alkenone reconstructions of subtropical North Atlantic surface hydrography and paleotemperature over the last 28 kyr, *Paleoceanography*, *11*, 343–358.

Charney, J. G. (1975), Dynamics of deserts and drought in the Sahel, *Q. J. R. Meteorol. Soc.*, *101*, 193–202.

Chase, Z., and R. F. Anderson (2004), Comment on "On the importance of opal, carbonate, and lithogenic clays in scavenging and fractionating ^{230}Th, ^{231}Pa and ^{10}Be in the ocean" by S. Luo and T.-L. Ku, *Earth Planet. Sci. Lett.*, *220*, 213–222.

Chase, Z., et al. (2002), The influence of particle composition and particle flux on scavenging of Th, Pa and Be in the ocean, *Earth Planet. Sci. Lett.*, *204*, 215–229.

Chou, C., et al. (2000), Ocean-atmosphere-land feedbacks in an idealized monsoon, *Q. J. R. Meteorol. Soc.*, *126*, 1–29.

deMenocal, P., et al. (2000a), Abrupt onset and termination of the African humid period: Rapid climate responses to gradual insolation forcing, *Quat. Sci. Rev.*, *19*, 347–361.

deMenocal, P., et al. (2000b), Coherent high- and low-latitude climate variability during the Holocene warm period, *Science*, *288*, 2198–2202.

Fleitmann, D., et al. (2003), Holocene forcing of the Indian monsoon recorded in a stalagmite from southern Oman, *Science*, *300*, 1737–1739.

Francois, R., M. Frank, M. M. Rutgers van der Loeff, and M. P. Bacon (2004), ^{230}Th normalization: An essential tool for interpreting sedimentary fluxes during the late Quaternary, *Paleoceanography*, *19*, PA1018, doi:10.1029/2003PA000939.

Ganopolski, A., et al. (1998), The influence of vegetation-atmosphere-ocean interaction on climate during the mid-Holocene, *Science*, *280*, 1916–1919.

Gasse, F. (2000), Hydrological changes in the African tropics since the Last Glacial Maximum, *Quat. Sci. Rev.*, *19*, 189–211.

Gasse, F., et al. (1990), The arid-humid transition in the Sahara and the Sahel during the last deglaciation, *Nature*, *346*, 141–146.

Hales, K., et al. (2004), Sensitivity of tropical land climate to leaf area index: Role of surface conductance versus albedo, *J. Clim.*, *17*, 1459–1473.

Haslett, S. K., and C. W. Smart (2006), Late Quaternary upwelling off tropical NW Africa: New micropalaeontological evidence from ODP Hole 658C, *J. Quat. Sci.*, *21*, 259–269.

Henderson, G. M., et al. (1999), Global distribution of the ^{230}Th flux to ocean sediments constrained by GCM modelling, *Deep Sea Res., Part 1*, *46*, 1861–1893.

Hodell, D., et al. (2001), Abrupt cooling of Antarctic surface waters and sea ice expansion in the South Atlantic sector of the Southern Ocean at 5000 cal yr B. P., *Quat. Res.*, *56*, 191–198.

Jolly, D., et al. (1998), Biome reconstruction from pollen and plant cacrofossil data for Africa and the Arabian peninsula at 0 and 6000 years, *J. Biogeogr.*, *25*, 1007–1028.

Jung, S. J. A., et al. (2004), Stepwise Holocene aridification in NE Africa deduced from dust-borne radiogenic isotope records, *Earth Planet. Sci. Lett.*, *221*, 27–37.

Kim, J. H., et al. (2002), Interhemispheric comparison of deglacial sea-surface temperature patterns in Atlantic eastern boundary currents, *Earth Planet. Sci. Lett.*, *194*, 383–393.

Kutzbach, J. E., and Z. Liu (1997), Response of the African monsoon to orbital forcing and ocean feedbacks in the middle Holocene, *Science*, *278*, 440–443.

Li, T., and S. G. H. Philander (1997), On the seasonal cycle of the equatorial Atlantic Ocean, *J. Clim.*, *10*, 813–817.

Liu, Z., et al. (2003), Coupled climate simulation of the evolution of global monsoons in the Holocene, *J. Clim.*, *16*, 2472–2490.

Luo, S., and T.-L. Ku (2004), On the importance of opal, carbonate, and lithogenic clays in scavenging and fractionating ^{230}Th, ^{231}Pa and ^{10}Be in the ocean, *Earth Planet. Sci. Lett.*, *220*, 201–211.

Magri, D., and I. Parra (2002), Late Quaternary western Mediterranean pollen records and African winds, *Earth Planet. Sci. Lett.*, *200*, 401–408.

Mayewski, P. A., L. D. Meeker, M. S. Twickler, S. Whitlow, Q. Yang, W. B. Lyons, and M. Prentice (1997), Major features and forcing of high-latitude Northern Hemisphere atmospheric circulation using a 110,000-year-long glaciochemical series, *J. Geophys. Res.*, *102*, 26,345–26,366.

Mercone, D., J. Thomson, I. W. Croudace, G. Siani, M. Paterne, and S. Troelstra (2000), Duration of S1, the most recent sapropel in the eastern Mediterranean Sea, as indicated by accelerator mass spectrometry radiocarbon and geochemical evidence, *Paleoceanography*, *15*(3), 336–347.

Mix, A. C., and W. F. Ruddiman (1986), Paleoceanography of the tropical Atlantic: 1. Spatial variability of annual mean sea-surface temperatures, 0–20,000 years B.P., *Paleoceanography*, *1*, 43–66.

Mortlock, R. A., and P. N. Frolich (1989), A simple method for the rapid determination of biogenic opal in pelagic marine sediments, *Deep Sea Res., Part A*, *36*, 1415–1426.

Muller, P. J., and G. Fischer (2001), A 4-year sediment trap record of alkenones from the filamentous upwelling region off Cape Blanc, NW Africa and a comparison with distributions in underlying sediments, *Deep Sea Res., Part 1*, *48*, 1877–1903.

Niyogi, D. S., et al. (2002), Hydrological land surface response in a tropical regime and a mid-latitudinal regime, *J. Hydrometeorol.*, *3*, 39–56.

Prahl, F. G., G. V. Wolfe, and M. A. Sparrow (2003), Physiological impacts on alkenone paleothermometry, *Paleoceanography*, *18*(2), 1025, doi:10.1029/2002PA000803.

Prell, W. L., and J. E. Kutzbach (1987), Monsoon variability over the past 150,000 years, *J. Geophys. Res.*, *92*, 8411–8425.

Ratmeyer, V., et al. (1999), Lithogenic particle fluxes and grain size distributions in the deep ocean off northwest Africa: Implications for seasonal changes of aeolian dust input and downward transport, *Deep Sea Res., Part 1*, *46*, 1289–1337.

Ritchie, J. C., et al. (1985), Sediment and pollen evidence for an early to mid-Holocene humid period in the eastern Sahara, *Nature*, *330*, 645–647.

Rohling, E. J. (1994), Review and new aspects concerning the formation of Mediterranean sapropels, *Mar. Geol.*, *122*, 1–28.

Rohling, E. J., and H. Palike (2005), Centennial-scale climate cooling with a sudden cold event around 8,200 years ago, *Nature*, *434*, 975–979.

Rohling, E. J., et al. (2003), Holocene atmosphere-ocean interactions: Records from Greenland and the Aegean Sea, *Clim. Dyn.*, *18*, 587–593.

Ruddiman, W. (1997), Tropical Atlantic terrigenous fluxes since 25,000 yrs B.P., *Mar. Geol.*, *136*, 189–207.

Sarnthein, M. (1978), Sand desserts during glacial maximum and climatic optimum, *Nature*, *271*, 43–46.

Shaw, T. J., and R. Francois (1991), A fast and sensitive ICP-MS assay for the determination of ^{230}Th in marine sediments, *Geochim. Cosmochim. Acta*, *55*, 2075–2078.

Shotyk, W., et al. (2002), A peat bog record of natural, pre-anthropogenic enrichments of trace elements in atmospheric aerosols since 12,370 ^{14}C yr BP, and their variation with Holocene climate change, *Earth Planet. Sci. Lett.*, *199*, 21–37.

Siani, G., et al. (2001), Mediterranean Sea surface radiocarbon reservoir age changes since the last glacial maximum, *Science*, *294*, 1917–1920.

Street, A. F., and A. T. Grove (1976), Environmental and climatic implications of late Quaternary lake-level fluctuations in Africa, *Nature*, *261*, 385–390.

Street-Perrott, F. A., and R. A. Perrott (1990), Abrupt climate fluctuations in the tropics: The influence of Atlantic Ocean circulation, *Nature*, *343*, 607–612.

Stuiver, M., and P. J. Reimer (1993), Extended 14C data base and revised CALIB 3. 0 14C age calibration program, *Radiocarbon*, *35*, 215–230.

Suman, D. O., and M. P. Bacon (1989), Variations in Holocene sedimentation in the North American basin determined from Th230 measurements, *Deep Sea Res.*, *36*, 869–878.

Waelbroeck, C., et al. (2001), The timing of the last deglaciation in North Atlantic climate records, *Nature*, *412*, 724–727.

Wang, G., and E. A. B. Eltahir (2000), Ecosystem dynamics and the Sahel drought, *Geophys. Res. Lett.*, *27*, 795–798.

Yu, E., et al. (2001), Trapping efficiency of bottom tethered sediment traps estimated from the intercepted fluxes of ^{230}Th and ^{231}Pa, *Deep Sea Res., Part 1*, *48*, 865–889.

Zeng, N., et al. (1999), Enhancement of interdecadal climate variability in the Sahel by vegetation interaction, *Science*, *286*, 1537–1540.

Zhao, M., N. A. S. Beveridge, N. J. Shackleton, M. Sarnthein, and G. Eglinton (1995), Molecular stratigraphy of cores off northwest Africa: Sea surface temperature history over the last 80 ka, *Paleoceanography*, *10*, 661–676.

J. Adkins, Department of Geological and Planetary Sciences, California Institute of Technology, 1200 E. California Boulevard, Pasadena, CA 91125, USA. (jess@caltech.edu)

P. deMenocal, Lamont-Doherty Earth Observatory of Columbia University, Geoscience 211, Route 9W, Palisades, NY 10964, USA.

G. Eshel, Department of Geophysical Sciences, University of Chicago, 5734 S. Ellis Avenue, Chicago, IL 60637, USA.